Capillary Condensation of Ionic Liquid Solutions in Porous Electrodes

Szparaga, Ryan; Woodward, Clifford E.; Forsman, Jan

Published in:
Journal of Physical Chemistry C

DOI:
10.1021/jp309794w

2013

Capillary Condensation of Ionic Liquid Solutions in Porous Electrodes.

Ryan Szparaga*, Clifford E. Woodward** and Jan Forsman*
*Theoretical Chemistry, Chemical Centre
P.O.Box 124, S-221 00 Lund, Sweden
**School of Physical, Environmental and Mathematical Sciences
University College, University of New South Wales, ADFA
Canberra ACT 2600, Australia

We use classical density functional theory to investigate room temperature ionic liquid + solvent mixtures in porous electrodes. We consider those mixtures that display a misicbility gap in the bulk fluid and hence have the capacity undergo capillary condensation in pores which preferentially attract the ionic liquid component. A novel aspect of this transition is that, when the system is at or near the critical point for this transition, we find an extraordinary increase in the capacitance, which derives from the fact that the capacitance is a thermodynamic response function, diverging at spinodal points.

PACS numbers:

I. INTRODUCTION

The ability of room temperature ionic liquids (RTILs) to screen charged surfaces is directly dependent upon their high density and short electrostatic screening lengths. These physical considerations, as well as their electrochemical stability, combine to make RTILs potential replacements for conventional electrolytes in devices such as electric double layer capacitors. On the other hand, the generally high viscosity of RTILs detracts from this potential, due to their poor kinetic response [1–4]. The addition of solvent to reduce the viscosity of RTILs and improve their dynamic performance has been suggested in the literature [1, 4, 5]. However, the addition of solvent would seem to remove many of the advantages of using a pure RTIL in particular, the ability to effectively screen surface charges on electrodes.

The advent of so-called porous carbon supercapacitors has been made possible by the ability to manufacture carbon-based porous materials [6]. These supercpacitors make use of the large electrode surface to volume ratio afforded by the many pores, which can be characterized by their mean diameter, D_p. Mesoporous carbon materials can be obtained via templating methods, giving pore sizes in the range 2nm $< D_p <$50nm and, so-called microporous materials contain even smaller pores. One would expect, however, a limit to the improvement in the capacitance obtained via increasing porosity. This is due to the diminishing ability of the electrolyte solution to screen the electrode charge as the average pore diameter decreases. That is, there is a free energy cost associated with the confinement of counterions in pores. This cost is dependent upon the nature of the bulk solution (from where the screening ions are sourced), as well as the size of the pore. The entropy of confinement of ions in pores, is manifested in repulsive electrode charge interactions, screened over a Debye length. For instance, if the pore size becomes less than the Debye length of the solution, one expects a significant free energy barrier will hinder screening of surface charges. The higher is the bulk ionic concentration, the lower is the entropy cost of confinement. If the pore size approaches the radius of the counter-ion (plus any hydration shell) then the ion size (steric length) becomes the relevant scale. For neat RTILs the Debye length and the steric length are similar. If additional attractive interactions are present in the pore, the free energy cost is reduced. An illustration of this is given by recent theoretical studies by Kondrat and Kornyshev [7] and Kondrat *et al* [8], which indicate that image forces in a conducting pore may be sufficient to induce a "superionic state" driven by attraction between the electrode walls and the counterions, as well as screening interactions between ions due to conductive electrons.

A decrease in capacitance with pore size has been shown to occur experimentally, with mesoporous carbon electrodes [9]. However, the capacitance in micropores (less than 1 nm) have been found to increase [9, 10]. As illustrated in recent simulations, the mechanism for this is possibly a structural one, driven by a combination of steric and electrostatic effects [11]. This mechanism has also been suggested by other theoretical work [12]. In the limiting case, extremely narrow micropores will be filled by counterions so that solvent and coions are completely excluded; the so-called electric wire in cylinder capacitor [13].

In a recent paper, we showed how efficient screening of electrode charges can be achieved by solutions containing RTILs, provided the latter are able to form wetting films at the electrode surface [14]. In the case of porous electrodes, surface wetting will likely be superseded by capillary condensation, especially for very narrow pores and/or attractive surfaces. In an RTIL+solvent mixture, charged pores can become laden with the ionic liquid in a phase concentrated relative to the solute in bulk. Below the bulk saturation concentration, capillary condensation may occur in pores when the free energy of the liquid-substrate interface is lower than the free energy of the

vapor-substrate interface [15, 16]. The degree to which the surface energy is lowered ultimately determines the pore widths, below which the concentrated phase will condense. Thus, the concentration at which capillary condensation occurs (for a given surface potential) depends upon the size of the pore, as well as its geometry. For geometries wherein the interface between dilute and concentrated phases is non-extensive, e.g., in cylindrical pores, the transition is a smooth one, becoming sharper as the pore radius increases. As described below, we will model pores as slits with area, S and separation H. In this case, the transition becomes sharp, as the interface grows as $S^{1/2}$, which is essentially allowed to become infinite.

Capillary induced condensation of an RTIL in a pore provides a low free energy path to very efficient screening of charged pores by RTIL+solvent mixtures. If the solvent species is less viscous than the neat RTIL, a better dynamic response of the mobile charge is also expected compared to the neat RTIL. One intriguing aspect of screening via phase transitions, is that sudden increases in the surface charge density at a particular potential are expected to occur. This provides a mechanism whereby a proportion of the capacitance charge can be delivered at a fixed voltage. Furthermore, this voltage can be 'tuned' by varying the average width of the electrode pores. As found in our previous work [14], we also find enhanced capacitances under supercritical conditions (close to the transition critical point). This is not surprising, as the differential capacitance is a thermodynamic response function that diverges at critical points.

The appearance of maxima in the differential capacitance, have been observed in other studies of electrochemical systems employing simple aqueous solutions. As in our case, these have been attributed to surface transitions [17]. For example, more than eighty years ago, Frumkin considered the effect on the differential capacitance of organic molecules adsorbed onto electrodes, and their displacement by water at large absolute potentials [18]. The work presented here is reminiscent of these earlier studies, albeit generalized to modern ionic liquids in the presence of porous electrodes. Recent theoretical work also deserves a mention. In particular, Kiyohara *et al* have performed constant potential Monte Carlo simulation on model porous electrodes [19–21]. For a simple primitive model electrolyte, those authors surprisingly observed a capillary condensation within the pores, as the potential difference was increased. The capillary induced phase separation (CIPS) observed in our current study occurs via a different mechanism to that observed in reference [19]. Nevertheless, similar effects on the differential capacitance should be seen in their work.

As far as we are aware, the implications of this type of surface transition on electrical properties, such as capacitance, have not yet been reported in the literature. We believe capillary condensation to be a more easily observed phenomenon in experimental studies than surface wetting. The ability to vary pore size and electrolyte concentration make for a very powerful combination of parameters, with which one may control the phenomenon. In this article, we shall use a classical density functional theory (DFT) to carry out a theoretical study, which will focus on capillary condensation of RTIL+solvent mixtures in model pores with slit-like geometries. A classical DFT for ionic liquids was recently reported by us to study oligimeric ionic liquids at interfaces [22]. Other approaches using the primitive model for electrolytes have also been reported in the literature[23]. One important feature of our modelling is the intrinsic asymmetry between anion and cation, which is neglected in simpler approaches. This asymmetry is manifest in the potential at which capillary condensation is manifested. This will be different in sign *and magnitude* when the cations are oligimeric and the anions are not. This also has implications for screening in very narrow pores, which may allow entry of the smaller ions only.

II. THEORY

This RTIL model has been described earlier [22], and a brief summary is given here. The cations are linear pentamers with a positive charge on the second monomer, the bond-length between spheres was chosen to be 5 Å. This model broadly mimics an imidazolium-based RTIL. The anions are negative spheres, representing simple species such as Cl^-. Of course, more elaborate models could have been used, but we would not expect them to change the qualitative features of our system dramatically. In our previous surface wetting study we used an implicit solvent model. Here we consider an explicit treatment of the solvent species. We envisage the (non-aqueous) solvent to be a molecular species. For simplicity, we assume that they have the same molecular structure as the oligomeric cations (pentamers) but without charge. Explicit solvent polarizability is omitted, entering only as an effective solvent dielectric constant, ϵ_r. All monomers, be they part of the oligomeric cations or solvent or the simple spherical cations interact with a Lennard-Jones (LJ) potential,

$$\phi_{\alpha\lambda}(r) = 4\epsilon_{\alpha\lambda}\left[(\frac{\sigma}{r})^{12} - (\frac{\sigma}{r})^{6}\right] \qquad (1)$$

where the distance r is measured from the centers of the monomers. In all cases we chose $\sigma = 5$ Å, equal to the bond length in the molecular species. The quantity, $\epsilon_{\alpha\lambda}$ is the interaction strength between species α and λ. We label all the monomers associated with ions with the subscript "i", whether they are charged or not. For example the the neutral monomers in the cation oligomer are labelled as such. Thus, all L-J interactions between RTIL monomers used $\epsilon_{ii} = 210kK$, where k is Boltzmann's constant. All calculations were performed at a temperature $T = 300K$. The solvent-solvent interactions, labelled as "s", are weaker: $\epsilon_{ss} = 140kK$. The Berethelot rule was adopted for cross interactions, i.e. $\epsilon_{is} \approx 171.46kK$.

The electrode pore is treated as a planar slit, with a charge per unit area equal to σ_s. The non-electrostatic interaction between the fluid monomers and a given surface were assumed to be an integrated Lennard-Jones potential,

$$\beta w_{w\lambda}(z) = 2\pi\epsilon_{w\lambda}\left[\frac{2}{45}(\frac{\sigma_{w\lambda}}{z})^9 - \frac{1}{3}(\frac{\sigma_{w\lambda}}{z})^3\right] \qquad (2)$$

where z is the perpendicular distance from the monomer center to the plane of charge and a single wall of the slit is labelled by the subscript "w". The surface interactions for the various monomer species were given by, $\epsilon_{wi} = 168kK$ and $\epsilon_{ws} \approx 137.2kK$; where the latter value follows from the first, by applying the Berthelot rules. Thus, the ions are assumed to adsorb more strongly to the surfaces than the solvent. In this work, we have assumed that the surfaces have a *uniform* charge density. For a perfectly conducting electrode one expects that this charge density is correlated with the free ions through image charges. Of course, most electrodes are not perfect conductors, and deviations are expected from the ideal image model for carbon electrodes say. This notwithstanding, as illustrated by Kondrat and Kornyshev [7], one expects that, for conducting electrodes, a correlated image charge will give rise to additional attractions between charged species and the electrode, arising from the ionic self-energy. In an effort to crudely mimic this extra attraction, we increased the Lennard-Jones interaction $w_{wi}/$, by an additional 25%. It should be noted that the overall qualitative results from our study here should be unchanged by this effect. Indeed, a more accurate, account of image self-energy, will only give rise to transitions occurring at somewhat different applied potentials. The screening of cross interactions between distinct ions, will also tend to facilitate capillary condensation. This effect is significant for very small pores only and we will ignore it in the present study

Capillary condensation of the RTIL+solvent mixture is essentially driven by surface interactions in addition to the electrostatic potential. These interactions cause demixing of the mixture within the pores, even when the bulk reservoir is under-saturated.

The Coulomb interaction between any two monomers, with charges q_α and q_λ is,

$$\Phi_{el}^{\alpha\lambda}(r) = \frac{1}{4\pi\epsilon_0\epsilon_r}\frac{q_\alpha q_\lambda}{r} \qquad (3)$$

where ϵ_0 is the permittivity of vacuum and ϵ_r is the relative dielectric constant of the solvent. In this study, we chose $\epsilon_r = 20$, which is typical of a number of non-aqueous solvents.

The functional describing the Helmholtz free energy (per unit electrode area), $\mathcal{F}$, for the RTIL+solvent mixture has been descibed in other references [22], but we describe it below for completeness. It can then be written as:

$$\begin{aligned}\beta\mathcal{F} &= \beta\mathcal{F}_p^{id}[N_c(\mathbf{R}), N_s(\mathbf{R})] + \int n_a(\mathbf{r})(\ln[n_a(\mathbf{r})] - 1)d\mathbf{r} + \\ &\beta\mathcal{F}_{hs}[\bar{n}_c(\mathbf{r}), \bar{n}_a(\mathbf{r}), \bar{n}_s(\mathbf{r})] + \\ &\int \beta w_{wi}(\mathbf{r})(n_c(\mathbf{r}) + n_a(\mathbf{r})) + \beta w_{ws}(\mathbf{r})n_s(\mathbf{r}))d\mathbf{r} + \\ &\frac{\beta}{2}\int\int{}' \sum_g\sum_d n_g(\mathbf{r})n_d(\mathbf{r}')\phi_{LJ}(|\mathbf{r}-\mathbf{r}'|)d\mathbf{r}d\mathbf{r}' + \\ &\frac{\beta}{2}\int\int \sum_\gamma\sum_\delta n_\gamma(\mathbf{r})n_\delta(\mathbf{r}')\Phi_{el}^{\gamma\delta}(|\mathbf{r}-\mathbf{r}'|)d\mathbf{r}d\mathbf{r}' + \\ &\int \sum_\gamma (w_{w\gamma}(\mathbf{r}) + V_{el}(\mathbf{r}) + f_{DHH}[\bar{n}_\gamma(\mathbf{r})])n_\gamma(\mathbf{r})d\mathbf{r} \quad (4)\end{aligned}$$

Here, sums with Roman and Greek letters run over L-J particles, and charged species, respectively. The prime above the L-J pair interaction integral, indicates that regions where $|\mathbf{r}-\mathbf{r}'| \leq \sigma$ should be excluded.

The ideal chain free energy, $\mathcal{F}_p^{id}[N_c(\mathbf{R}), N_s(\mathbf{R})]$ of the cations and the solvent can be exactly expressed as a functional of the oligomer distributions $N_i(\mathbf{R})$, where $\mathbf{R} = (\mathbf{r}_1, ..., \mathbf{r}_5)$ with $\mathbf{r}_i$ the coordinate of monomer i [24, 25]. The hard sphere exclusion free energy, $\mathcal{F}_{hs}$, results from an integration of a Generalized Flory-dimer equation of state [26–29]. The weighted cation density, $\bar{n}_m(\mathbf{r})$, is given by [30]: $\bar{n}_c(\mathbf{r}) = (3/4\pi\sigma^3)\int n_c(\mathbf{r}')\Theta(|\mathbf{r}-\mathbf{r}'|-\sigma)d\mathbf{r}'$, where $\Theta(x)$ is the Heaviside step function. The other coarse-grained densities, $\bar{n}_a(\mathbf{r})$ and $\bar{n}_s(\mathbf{r})$, are obtained in a similar fashion. The potential from the uniformly charged electrode is denoted V_{el}. Electrostatic correlations are approximated by the functional f_{DHH}, borrowing concepts from the "hole corrected Debye-Hückel" theory [31–33] for the one-component plasma. The correlation free energy per charged particle particle α is given by

$$\begin{aligned}4\beta f_{DHH}[\bar{n}_\alpha(\mathbf{r})] &= 1 + \frac{2\pi}{3\sqrt{3}} - \ln[3] + \ln[\omega^2+\omega+1] - \\ &\omega^2 - \frac{2}{\sqrt{3}}\tan^{-1}[\frac{2\omega+1}{\sqrt{3}} \qquad (5)\end{aligned}$$

where $\omega = [1 + c\bar{n}_\alpha^{1/2}]^{1/3}$ and $c = |\frac{q_\alpha}{e}|^3(3l_B)^{3/2}\sqrt{\frac{4\pi}{3}}$. The Bjerrum length is, $l_B = e^2\beta/(4\pi\epsilon_0\epsilon_r)$.

We assume that the fluid within the pore is in chemical equilibrium with a surrounding bulk solution. Thus, it is appropriate to use the grand potential,

$$\Omega = \mathcal{F} - \sum_i \{\mu_i + q_i\psi_D\}N_i \qquad (6)$$

Note that in this expression we sum over all particles both neutral and charged. μ_i is the chemical potential of the i^{th} species (with charge q_i and number N_i) and ψ_D is the Donnan potential, which maintains electro-neutrality in the pore. The free energy functional, ω, is minimized with respect to the IL and solvent density profiles, for

each chosen surface charge density (with fixed bulk solution conditions). The symmetry of the system allows the (x, y) dimensions, parallel with the surfaces, to be integrated out, leaving z dependend quantities. The mean-field electrostatic interactions (save the correlation part, see above) is handled in a standard Poisson-Boltzmann manner, wherein electroneutrality is ensured via a Donnan potential. The free energy functional minimization is numerically achieved via Picard iterations, utilizing auxiliary monomer density fields, $c(i, z)$. These are progressively calculated (increasing i), via a repeated series of Boltzmann weighted bond integrals (i.e. across spherical surfaces, with radius σ), as described in detail, in previous works [34]. The end monomer field then provides the Boltzmann weighted probability for an $i-1$-mer to be connected with end i, located at position z. The final probability for monomer i to be located at z is obtained as a product of the two end probability fields, $c(i, z)$ and $c(6-i, z)$ (with our pentamer cation and solvent molecule models). If we specifically consider the cationic pentamers, the total monomer density profil is provided by a sum of monomer contributions along the chain (ρ_p^b is the bulk pentamer density):

$$n_m(z) = \rho_p^b \sum_{i=1}^{5} c(i, z)c(6-i, z) \tag{7}$$

$c(i, z)$ fulfills a recursive relation, $c(1, z) = 1$ and for $i \in [2, 5]$:

$$c(i, z) = e^{\lambda_{i,b}} \int c(i-1, z')T_{i,i-1}(z', z)dz' \tag{8}$$

where the connectivity matrix $T_{i,i-1}(z', z)$ is defined in terms of the excess monomer free energies $\lambda_i(z)$ ($\lambda_{i,b}$ is the bulk value):

$$T(z', z) = \frac{1}{2\sigma} e^{-\lambda_i(z)/2} \Theta(|z - z'| - \sigma) e^{-\lambda_{i-1}(z')/2} \tag{9}$$

$$\lambda_i(z) = \frac{\delta \mathcal{F}[n(z)]}{\delta n_i(z)} \tag{10}$$

We note that the the second monomer requires special consideration (different local field, λ), as it is charged.

In experimental set-ups one can have the situation where the porous electrode is held at constant potential relative to the bulk. In this case the surface charge will fluctuate and the grand potential should be appropriately generalized,

$$\Omega = \mathcal{F} - \sum_i \{\mu_i + q_i \Psi_D\} N_i - 2S\sigma_s \Psi_s \tag{11}$$

Here Ψ_s is the surface potential.

III. RESULTS

With the potential parameters chosen above, the free energy functional was minimized for the RTIL+solvent mixture in the bulk. The system display a miscibility gap in the bulk fluid, with coexistence between phases contianing high and low concentrations of the RTIL. The upper solution critical temperature is 314.5 K, i.e. about 5% higher than the temperature (300K) of our investigated systems. All calculations were made at a pressure of 1 bar. At 300 K, the dilute phase, that coexist with a concentrated phase in the bulk, has an IL salt concentration of $\rho_{cat}\sigma^3 \approx 0.018$, and a solvent density of $\rho_{solv}\sigma^3 \approx 0.059$. The corresponding values for the concentrated phase are $\rho_{cat}\sigma^3 \approx 0.060$, and $\rho_{solv}\sigma^3 \approx 0.0315$.

A. Single Electrode

We studied the behaviour of these phases in the presence of a single electrode. A similar system was studied by us in previous work [14], albeit with an implicit solvent model. In that work, we established the possibility of prewetting of the surface by the concentrated phase, when the electrode was in contact with an undersaturated bulk solution. In the present study, we are outside the prewetting regime. Figure 1 (a), shows the density profiles of the cationic and solvent monomers against a neutral surface, for a bulk fluids at the concentrated branch, and at 10 % undersaturation (dilute), respectively. By "monomers" we refer the connected spheres, of diameter σ, that buid up the cations and solvent molecules, in our coarse-grained models. The displayed total "monomer" density is the sum of all monomeric contributions, for the respective oligomeric molecules. Due to cooperativity effects, brought about by connectivity, these will in general display a stronger surface affinity than the "single-sphere" (purely monomeric) anions. Thus, the adsorption of cation oligomers is somewhat hampered by electrostatic repulsions, due to the limited adsorption of anions. While this is not immediately apparent when the bulk is undersaturated, it is clearly the case for a concentrated solution. In this case we see that the adsorption of solvent remains strong, in comparison to the cations, even though the latter are more than twice as concentrated in the bulk phase. Indeed the cationic monomers seem to display a "depleted" density profile, due to the excluding effect of strongly adsorbed solvent. This profile is quite different to that of the cations in a the neat RTIL , Figure 1 (b). There is much interest in the capacitance of electrodes immersed in RTILs. The differential capacitance is defined as:

$$\begin{aligned} C_D &= \partial\sigma_s/\partial\psi_s \\ &= \partial^2\Omega/\partial\Psi_s^2 \end{aligned} \tag{12}$$

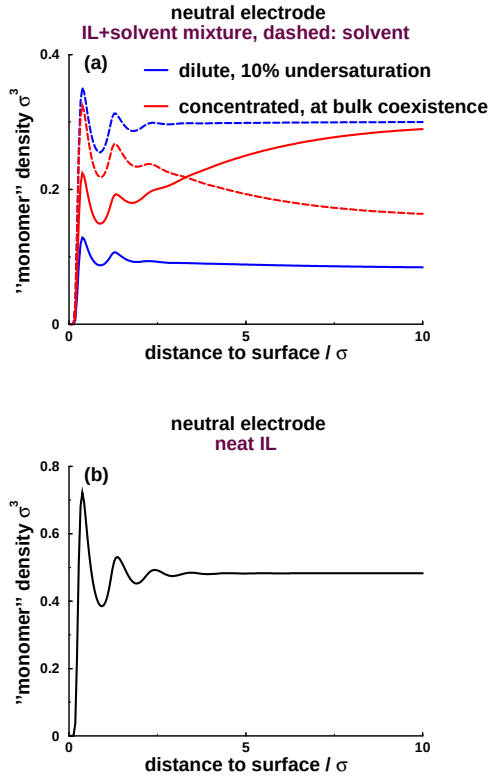

FIG. 1: Density profiles of cation (solid line), and solvent (dashed), monomers at a single neutral electrode. Note that the displayed profiles are the sums of *all* monomer contributions, within the oligomeric molecules, as obtained via a numerical free energy minimization scheme (see main text). (a) RTIL+solvent mixtures. The concentrated and dilute branch solutions are displayed. In the former case, bulk conditions are at coexistence, whereas the dilute phase has an IL concentration 10 % below the bulk coexistence value. (b) Neat RTIL, at the same pressure and temperature (1 bar, 300 K).

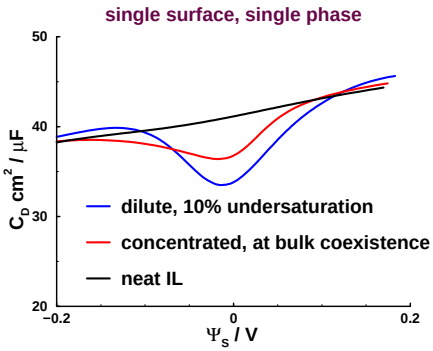

FIG. 2: Differential capacitance against a single charged electrode, as a function of the applied voltage and for varying bulk conditions. The curves, as labelled, correspond to the bulk densities described in Figure 1.

Figure 2 shows the differential capacitance against a single electrode, as a function of the surface voltage, for the different solution densities described above. The appearance of "camel-shaped" capacitances is well-known in experiments and has been observed in a number of theoretical treatments [35–39]. We have shown in previous work, that, for neat RTILs, the dispersion interaction between the fluid and the electrode surfaces can play a major role in establishing the characteristic dip of C_D at low voltages [40]. We also showed that, for strongly adsorbing surfaces, this feature can be reduced or made to disappear. Such is the case in the present study, wherein the neat RTIL displays no such dip, due to the strong surface interaction with the ions. Note that in this figure, we have focused only on the region around zero potential. For very large (absolute) potentials, the differential capacitance will decrease, due to excluded volume effects. The behaviour of the neat RTIL, can be contrasted with that of the RTIL mixtures, which show the "camel-shaped" profiles, even for adsorbing surfaces. The reason for this is the competitive adsorption of the solvent and the ions. For weak potentials, the solvent adsorbs more strongly and the surface capacitance is small. However, for increasing surface potential, the solvent is displaced by screening ions, and the capacitance increases. Finally, excluded volume effects will dominate at very large (absolute) potentials, causing C_D to decrease again. Thus, the theoretical work presented here, suggests yet another mechanism for producing camel-shaped capacitances in the presence of contaminating species, which may compete for surface adsorption with the ions.

B. Capillary Condensation

In the case of an undersaturated bulk solution, the dilute phase is the thermodynamically preferred state. However, in the presence of a porous electrode, which is attractive to the ions, it is possible that capillary condensation may occur. In our model, a pore consists of two parallel, planar electrode surfaces, held a fixed distance, H, apart. We treat single pores, characterized by a surface charge per unit area, σ_s, on both surfaces. The potential zero was again assumed to be in the bulk. We found that for a single pore it was possible to obtain capillary induced phase separation (CIPS) for both positive and negative surface potentials. In the former case, the condensation is driven by adsorption of anions, and in the latter case by the cations. The onset of capillary condensation in the pore is a due to the lower surface tension between the concentrated phase and the charged electrode, compared with that of the dilute phase. For small enough H, the correlation length in the fluid is sufficient to prevent the formation of a wetting layers (adjacent to

the electrodes), in preference to capillary condensation. Of course, for wider pores, the formation of wetting layers become more likely. At a particular value for the

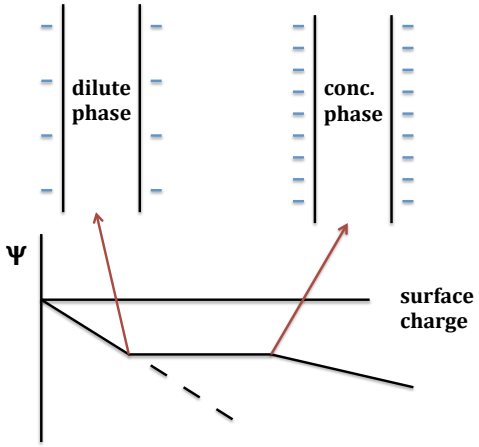

FIG. 3: Schematic diagram showing the variation in surface potential versus surface charge density in a pore, in the part of the phase diagram which displays a transition between dilute and concentrated phases in the pore - a capillary induced phase separation, CIPS. Note the jump in the surface charge density at a fixed potential at the point of the transition, which gives rise to an infinite differential capacitance

applied potential, the dilute and concentrated phase are at coexistence in the pore. The associated surface charge densities will be dfferent for the two phases, see Figure 3. Further increasing the *magnitude* of the applied potential will favour the concentrated phase, while the dilute phase becomes metastable. For a strong enough applied potential, the dilute phase will become unstable, passing through a spinodal point. A spinodal point represents the limit of stability of a phase, and is characterized by divergences in response functions, such as the differential capacitance. The concentrated phase, can also display spinodal behaviour. Figure 4 shows the effect on the differential capacitance for negative surface potentials at a given degree of bulk undersaturation and pore width. At very negative potentials the concentrated phase has condensed in the pore, driven by the excess adsorption of the oligomeric cations. As the magnitude of the potential is reduced the condensed phase eventually becomes unstable, as indicated by the divergence of C_D at an *upper* spinodal point. Beyond this point the dilute phase is the only stationary solution to the free energy functional. On the other hand, reversing the potential path by beginning with the dilute phase and going toward more negative potentials, we pass through a *lower* spinodal point separating the dilute and concentrated phases. The difference in potentials at the upper and lower spinodals indicate hysteresis, which is typical for first-order transitions. These potential values of course bracket the point of coexistence between dilute and concentrated phases in

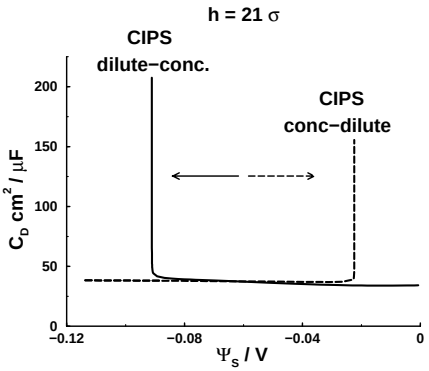

FIG. 4: Differential capacitance, C_D, versus surface potential for a charged pore with H/σ = 21. The bulk ionic density is $\rho_{cat}\sigma^3 = 0.018$, which is slightly below the bulk coexistence value of $\rho_{cat}\sigma^3 \approx 0.01836$ The dotted curve shows the result of starting at a stable concentrated phase in the pore at large negative potentials, and procedding to lower the magnitude. Eventually the system reaches a spinodal point, where C_D become infinite. Hysteresis is displayed by starting the system in the stable dilute phase at zero surface potential, and increasing the magnitude of a negative potential. The second spinodal between dilute and concentrated phases is reached at a lower (more negative) potential than the first.

the pore.

C. Supercritical Behaviour

One may obtain better dynamic performance of the condensed liquid in porous electrodes, compared with that of the neat ionic liquid, especially when the bulk is quite dilute. However, the presence of a first-order phase change and accompanying hysteresis may still make the response somewhat sluggish. Hence, it is also of interest to explore the behavior the fluid under slightly supercritical conditions. Here one still expects to find large fluctuations in the system (close to the critical point). Thus, the capacitance will become large at particular values of pore size and potential, while the electrodes will be expected to discharge relatively quickly in the absence of a first-order phase change. The phase diagram in the pore can be considered as a function of the pore width H and the degree of undersaturation in the bulk. Varying the applied potential will produce a line of (pore) critical points, as shown in Figure 5. In Figure 6, we show the effect of varying the bulk IL concentration on C_D. It is instructive to note firstly, the enormous increase in the capacitance over a narrow potential window, due to the proximity of the critical point in the pore. As a general rule of thumb, we can state that the fluctuation enhancement in C_D is greater the closer the system parameters are to the line of critical points. It is clear that a more undersaturated bulk is further from the line of

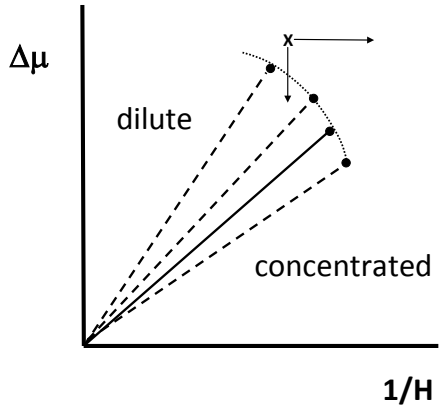

FIG. 5: Schematic phase diagram for capillary condensation, as a function of the inverse pore width and the degree of undersaturation $\Delta\mu$. The solid curve represents the line of first-order phase transitions for a neutral pore, terminating at a critical point. The dotted lines represent the shift in this phase boundary as the surface potential is varied. All lines terminate at critical points. For slightly negative potentials, the critical point shifts to lower $\Delta\mu$ and H. As the magnitude of the potential increases, the critical points reverse direction and head toward larger H and $\Delta\mu$. The point 'x' marks a particular supercritical point. We see that decreasing H moves it away from the line of critical points, as would increasing $\Delta\mu$. On the other hand, increasing the bulk density can cause the phase point to cross the line of critical points into the first-order regime.

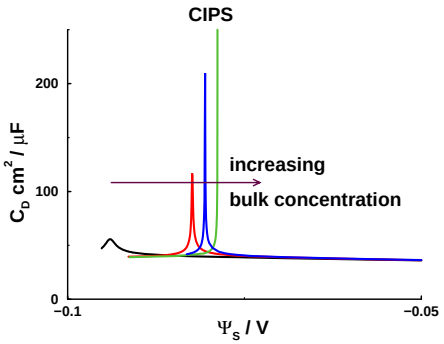

FIG. 6: Differential capacitance, C_D, versus surface potential for a charged pore with H/$\sigma = 12.4$ under supercritical conditions. The peaks in the capacitance is indicative of a nearby critical point. The profiles for several values of the bulk density are shown, $\rho_{cat}\sigma^3 = 0.0164$, 0.0166, 0.0167 and 0.0168. The corresponding solvent densities were as usual given by the constraint from a bulk pressure of 1 bar. By decreasing the degree of undersaturation, capillary induced phase transition can be induced in the system.

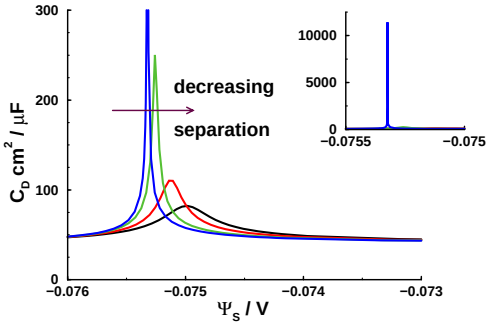

FIG. 7: Differential capacitance, C_D, versus surface potential for a charged pore with $\rho_{cat}\sigma^3 = 0.0170$, $\rho_{sol}\sigma^3 \approx 0.060$. under supercritical conditions. The pore width is varied, $H/\sigma = 12.25$, 12.2, 12.1 and 12. Decreasing the separation takes the system further from the line of critical point, depicted in Figure 5

critical points, while decreasing the degree of undersaturation may eventually leads to a first-order transition. On the other hand, varying the pore width will also lead to movement either away or toward the critical line, see Figure 7. This fact has implications in real experimental systems, where one expects to find electrode with a variety of pore diameters. It suggests that a fluctuation enhanced differential capacitance will be observed over a large potential range, due to the population of pores. Furthermore, one should be able to choose the potential at which one sees the this enhanced capacitance, by control of the pore width distributions.

IV. CONCLUSIONS

The work presented here investigates the behaviour of a coarse-grained model for an RTIL+solvent mixture in the presence of planar pores. The qualitative behaviour is not expected to change for other pore geometries, though transitions may become non-sharp in cases such as cylindrical pores, wherein the interface between coexisting phases does not scale with a size parameter. The advantages of using RTIL+solvent mixtures in supercapacitors are manifold. An obvious example is the decrease in the electrolyte viscosity (due to the presence of a lower viscosity solvent), which would improve the response time of electrochemical devices compared to neat RTILs. Our work has focused on capillary condensation in such a system, which can give rise to fluctuation enhanced capacitance over a range of surface potentials. This increase in capacitance is due to density fluctuations in the screening electrolyte, associated with that transition. Even under supercritical conditions one observes enhanced capacitance if the critical point is nearby in the parameter space. We concluded that in actual electrodes, the nat-

ural inhomogeniety in pore widths will likely guarantee that a sub-class of surface environments will show fluctuation enhanced capacitance, as the system traverses a range of surface potentials. The possibility that surfaces can be engineered to display enhanced capacitances over a specific potential window is an exciting possibility, which suggests that capacitors may be induced to act more like batteries, delivering most of their power at a given potential. Such concerns have already been considered by Kondrat *et al* in recent work [35] and results reported here may add another level of flexibility to supercapacitor design.

Our study here is somewhat idealized, in that we only consider a single electrode pore immersed in a bulk electrolyte. As stated above, in an actual capacitor, the electrodes would contain many pores, described by different values of H (assuming planar shapes, which of course may not be the case). Furthermore, the relevant electrostatic potential is that which exists between the two electrodes. This would imply that pores with different width would carry different surface charges (so as to maintain a given potential). Finally, the total surface charges on the opposing electrodes would be equal in magnitude and opposite in sign. While the study pursued here investigated the behaviour of isolated constituent pores, we propose to study a more realistic scenario of connected electrodes exhibiting a range of pore sizes. In such a system, the total free energy will consist of a sum of the separate electrode free energies, linked by the electro-neutrality constraint on their charges. The free energy contribution for each electrode will be obtained as a sum over seperate pore sizes, weighted by their distribution. Such a study will allow us to investigate the role of pore size distribution on electrode capacitance.

[1] R. Reddy, J. Phase. Equilib. Diffus. **27**, 3 (2006).
[2] E. Frackowiak, G. Lota, and J. Pernak, Appl. Phys. Lett. **86**, 164104 (2005).
[3] E. Frackowiak, Phys. Chem. Chem. Phys. **9**, 1774 (2007).
[4] K. Lovelock, F. Cowling, A. Taylor, P. Licence, and D. Walsh, J. Phys. Chem. B **114**, 4442 (2010).
[5] N. Khupse and A. Kumar, J. Solution Chem. **38**, 589 (2009).
[6] A. Shukla and T. Prem Kumar, Wiley Interdisciplinary Reviews: Energy and Environment (2012).
[7] S. Kondrat and A. Kornyshev, J. Phys.: Cond. Matter **23**, 022201 (2011).
[8] S. Kondrat, N. Georgi, Fedorov, and A. A. Kornyshev, Phys. Chem. Chem. Phys. **13**, 11359 (2011).
[9] J. Chmiola, G. Yushin, Y. Gogotsi, C. Portet, P. Simon, and P. Taberna, Science **313**, 1760 (2006).
[10] C. Largeot, C. Portet, J. Chmiola, P.-L. Taberna, Y. Gogotsi, and P. Simon, J. Am. Chem. Soc. **130**, 2730 (2008).
[11] P. Wu, J. Huang, V. Meunier, B. Sumpter, and R. Qiao, ACS Nano **5**, 9044 (2011).
[12] D.-e. Jiang, Z. Jin, and J. Wu, Nano Letters **11**, 5373 (2011).
[13] J. Huang, B. Sumpter, and V. Meunier, Chem. Euro. J. **14**, 6614 (2008).
[14] R. Szparaga, C. E. Woodward, and J. Forsman, J. Phys. Chemi. C **116**, 15946 (2012).
[15] R. Evans, U. Marconi, and P. Tarazona, J. Chem. Phys. **84**, 2376 (1986).
[16] J. Forsman and W. C.E., Mol. Phys. **90**, 637 (1997).
[17] A. Kornyshev and I. Vilfan, Electrochimica Acta **40**, 109 (1995).
[18] Frumkin, Z. physikal. Chem **111**, 190 (1924).
[19] K. Kiyohara, T. Sugino, and K. Asaka, The Journal of Chemical Physics **134**, 154710 (2011).
[20] K. Kiyohara, T. Sugino, and K. Asaka, The Journal of Chemical Physics **132**, 144705 (pages 12) (2010).
[21] K. Kiyohara and K. Asaka, The Journal of Physical Chemistry C **111**, 15903 (2007).
[22] J. Forsman, C. Woodward, and M. Trulsson, J. Phys.Chem. B **115**, 4606 (2011).
[23] D. en Jiang, D. Meng, and J. Wu, Chemical Physics Letters **504**, 153 (2011).
[24] C. Woodward, J. Chem. Phys. **94**, 3183 (1991).
[25] C. Woodward, J. Chem. Phys. **97**, 695 (1992).
[26] J. Wichert, H. Gulati, and H. C.K., J. Chem. Phys. **105**, 7669 (1996).
[27] J. Forsman, C. Woodward, and B. Freasier, J. Chem. Phys. **117**, 1915 (2002).
[28] J. Forsman and C. Woodward, J. Chem. Phys. **120**, 1506 (2004).
[29] J. Forsman and C. Woodward, J. Chem. Phys. **119**, 1889 (2003).
[30] S. Nordholm, M. Johnson, and B. Freasier, Aust. J. Chem. **33**, 2139 (1980).
[31] S. Nordholm, Chem. Phys. Letts. **105**, 302 (1984).
[32] R. Penfold, S. Nordholm, B. Jönsson, and C. Woodward, J. Chem. Phys. **92**, 1915 (1990).
[33] R. Penfold and S. Nordholm, J. Chem. Phys. **95**, 2048 (1991).
[34] J. Forsman and C. E. Woodward, Macromol **40**, 8396 (2007).
[35] S. Kondrat, C. R. Perez, V. Presser, Y. Gogotsi, and A. A. Kornyshev, Energy Environ. Sci. **5**, 6474 (2012).
[36] S. Lamperski, C. W. Outhwaite, and L. B. Bhuiyan, The Journal of Physical Chemistry B **113**, 8925 (2009).
[37] S. Lamperski and D. Henderson, Molecular Simulation **37**, 264 (2011).
[38] D. Henderson, S. Lamperski, Z. Jin, and J. Wu, The Journal of Physical Chemistry B **115**, 12911 (2011).
[39] M. V. Fedorov and A. A. Kornyshev, The Journal of Physical Chemistry B **112**, 11868 (2008).
[40] M. Trulsson, J. Algotsson, J. Forsman, and C. E. Woodward, J. Phys. Chem. Lett. **1**, 1191 (2010).